Journal of Power Sources 226 (2013) 112–121

Contents lists available at SciVerse ScienceDirect

Journal of Power Sources

journal homepage: www.elsevier.com/locate/jpowsour

Optimization of ink composition based on a non-platinum cathode for single membrane electrode assembly proton exchange membrane fuel cells

K. Artyushkova*, D. Habel-Rodriguez, T.S. Olson, P. Atanassov

Center for Emerging Energy Technologies, Chemical and Nuclear Engineering Department, University of New Mexico, Albuquerque, NM 87131, USA

HIGHLIGHTS

- ► Effect of catalyst ink formulation on performance and stability is studied.
- ► XPS is used to study surface chemistry of various ink formulations.
- ► Statistical structure-to-property relationship is built by PCA.
- ► Better performance is linked to pyridinic N, N bounded to Co and CoO particles.
- ► Higher stability is associated with preserved moieties from carbon black and ionomer.

ARTICLE INFO

Article history:
Received 31 August 2012
Received in revised form
15 October 2012
Accepted 18 October 2012
Available online 26 October 2012

Keywords:
Non-platinum electrocatalysts
Oxygen reduction reaction
MEA stability
XPS
Structure-to-property relationship
Multivariate analysis

ABSTRACT

Non-Pt based oxygen reduction catalyst H_2-air fuel cell performance is reported for various electrode compositions. Ink formulations for pyrolyzed Co porphyrin based cathode electrocatalysts were evaluated in a membrane electrode assembly (MEA) configuration and X-ray photoelectron spectroscopy was performed on the MEA catalyst layers. The effect of cooling time trajectories of the catalysts after pyrolysis as well as Nafion content in the ink formulation were studied. By building statistical structure-to-property relationships between XPS and MEA performance using multivariate analysis we have determined that the higher stability of fast-cooled containing inks is mainly associated with better preserved graphic carbon from the carbon black and C–F moieties of the Nafion, while better MEA performance is a result of the presence of these moieties as well as pyridinic nitrogen and nitrogen associated with metal in the pyropolymer. Optimal Nafion content is determined at 1:1 catalyst:Nafion weight ratio, while higher Nafion concentrations causes oxidation of the Nafion backbone itself as well as leaching of the Co_xO_y particles from the catalyst and formation of oxidized species of Co, O, C and F. Further, we report 1500 h of continuous fuel cell operation for two different non-platinum cathode catalysts in the optimized MEA.

1. Introduction

Proton exchange membrane fuel cells (PEMFC) and direct methanol fuel cells (DMFC) use platinum-based electrocatalysts in both the anode and cathode. Since platinum is both expensive and of limited availability, there is a need for developing and optimizing non-platinum based catalysts in order for fuel cells to be competitive with alternative energy conversion technologies. Non-platinum-based catalysts such as pyrolyzed macrocycles are a less active but inexpensive alternative material that could be used in larger quantities to meet the same power demands. The use of macrocycles as electrocatalysts has been studied for their unique catalytic properties since the 1960s. [1] More recently there have been a number of publications presenting MEA performance data using a non-platinum-based cathode catalyst [2–7].

Non-precious metal based catalysts are optimized differently than platinum-based catalysts, where for the former one strives for maximum catalyst loading, and for the latter one needs to use ultra-low metal loadings due to the cost. Freed from the constraint of the price of the catalyst metal, the best designs for non-precious metal based catalysts maximize both the number of catalytically active sites for oxygen reduction as well as the reactant transport through the catalyst layer in MEAs. Gasteiger et al suggested that if the catalyst may be consider costless, performance can be measured in volumetric currents (A cm^{-3}) with the volume depending on thickness of the catalyst layer and the geometric area of the MEA [8]. In our previous report we evaluated the H_2/air–O_2 MEA performance for different catalyst layer compositions utilizing

* Corresponding author. Tel.: +1 505 277 0750; fax: +1 505 277 5433.
E-mail address: kartyush@unm.edu (K. Artyushkova).

0378-7753/$ – see front matter © 2012 Elsevier B.V. All rights reserved.
http://dx.doi.org/10.1016/j.jpowsour.2012.10.062

a templated non-platinum oxygen reduction reaction (ORR) catalyst based on porphyrin macrocycles [5]. The effect of the non-platinum catalyst, Nafion, and 35 wt% Teflon modified Vulcan XC-72 Carbon Black (XC-35) loadings were measured under H_2/air and H_2/O_2 conditions. Transport hindrances that occur in the catalyst layers were evaluated with *E* vs. *i* analysis. It was shown that transport limitations in the cathode catalyst layer can limit the performance of the cell at relatively low current densities if the catalyst layer composition is not optimized.

Large-scale deployment of PEMFCs is facing another major challenge: increase of the lifetime. One way to improve durability is to maintain the chemical integrity, and hence, effectiveness of the catalyst layer (CL) over the lifetime of the fuel cell. CL durability is of key importance, and methodologies for improving it are being intensively pursued. CL degradation is linked to catalyst dissolution and agglomeration, ionomer degradation, carbon support degradation, and the degradation of pore morphology and surface properties [9–13].

In case of non-platinum-based, the catalyst layer is comprised of carbon particles supporting the templated catalyst. For high performance, the CL requires a sufficiently contiguous carbon matrix for good electron conductivity, and adequate surface availability of catalytically active centers for fuel/oxidant adsorption, dissociation, and electrochemical reactions. In addition, the CL must provide sufficient ionomer for proton transport, and adequate pore space for the transport of both reactant gases and removal of product water.

Although Nafion®, which is a conventionally used ionomer in PEMFCs, has demonstrated a high efficiency and a stable performance in fuel cell applications; evidence of membrane degradation is reported [14]. It is believed that membrane degradation is mainly caused by chemical attack of the polymer [12,14]. Effect of Nafion on the CL durability on non-PGM (Platinum-group metals) containing systems is under-investigation and is of critical importance in advancing the technology.

Commonly used electrochemical and other methods to investigate degradation of the CL and membrane have failed to detect the ionomer degradation in the catalyst layer. X-ray photoelectron spectroscopy (XPS) is a powerful technique to study the chemical changes in the polymer membrane. It has been applied to quantitatively analyze catalyst layer degradation in PEM fuel cells. XPS was shown to be very useful for determining both the elemental concentrations and chemical states of C, F, Pt, O and S on the catalyst layer [11,13,14]. It has been shown that the ionomer on the catalyst layer dissolves and/or decomposes, and that characteristic XPS signals decrease after about 300 h of fuel cell operation. Ionomer degradation was characterized by a decrease of CF_3 and CF_2 species and an increase in oxidized forms of carbon (e.g. C–O and C=O).

In the current report we study the effect of catalyst preparation and ink composition on MEA performance and stability by XPS. We report 1500 h of operation for non-platinum containing cathode in MEA. By building structure-to-property relationship between XPS and MEA testing data using multivariate analysis we determine which types of chemical structures and which types of ink formulations result in better performance and better stabilities.

2. Experimental

2.1. Catalyst preparation

Catalyst porphyrin precursor CoTMPP (Co-tetramethoxyphenylporphyrin) was obtained from Aldrich Chemical Company (CAS 28903-71-1) and was used without further purification. Cab-O-Sil M-5, an amorphous fumed silica (325 $m^2\ g^{-1}$ specific surface area) obtained from Cabot Corporation, was used as the carrier. The organic solvent was tetrahydrofuran, 99.99% assay by gas chromatography, obtained from EM Science (Merck). A Lindberg Blue tube furnace with a programmable controller was used in the pyrolysis process with 99.9% pure nitrogen which was obtained from local sources. 0.5 g of porphyrin sample was weighed and dissolved in tetrahydrofuran and mixed with 0.5 g of amorphous fumed silica and sonicated for 15 min for uniform dispersion of silica in the solution matrix. The templated material was then pyrolyzed at 700 °C for 4 h under nitrogen gas flow. An adequate flow of nitrogen is supplied to provide an inert residence environment, which prevents oxidation of organics at the high temperatures. Two types of cooling were employed: slow-cooled (cooling rate 3 K min^{-1}) and fast-cooled (estimated cooling rate 20 K min^{-1}). The sample was stirred with 7.0 M KOH to etch out the silica. Finally, the sample was washed with (de-ionized) DI water and dried.

2.2. Ink fabrication

The standard anode ink was prepared as follows: 40 mg of PtRu black, 500 mg DI H_2O, and 166 mg of 5% Nafion solution was sonicated and hand painted on an 1135 Nafion membrane.

The non-platinum cathode inks were prepared as follows: 4 mg cm^{-2} geometric CoTMPP catalyst was mixed with a 20 wt% Teflon/Vulcan XC-72 (noted here as XC-35) material and 1:0.5, 1:1, 1:2 and 1:3 5% catalyst:Nafion weight ratio. Cathode inks were analyzed by XPS as is by drying them on the sample bar.

2.3. MEA fabrication and testing

The non-platinum cathode ink was then hand painted on an 1135 Nafion membrane (Ion Power) and the microporous layer of the gas diffusion layer (GDL LT 1400-W Low temperature, ELAT(R) GDL microporous layer on woven web) in a ratio of 1:9, respectively. The MEA was then pressed at 345 N cm^{-2} at 125 °C for 10 min.

The MEA was placed in a 5 cm^2 cell with serpentine flow channels and the bolts were compressed to 553 kPa (80 lb in^{-2}). The fuel cell technologies fuel cell test station was used to obtain H_2/O_2 and H_2/air polarization curves. Polarization curves were obtained galvanostatically with a 30 s delay before data acquisition. The anode and cathode gases were heated and humidified at 85 °C, and the flow rates were 266 and 466 sccm, respectively. The cell operating temperature was maintained at 80 °C. Polarization curves were acquired at 0 and 20 N cm^{-2} backpressure.

2.4. HRTEM

TEM was performed on a JEOL 2000 FX microscope operating at 200 keV.

2.5. XPS analysis

The XPS spectra were acquired using a Kratos AXIS Ultra photoelectron spectrometer equipped with a monochromatic Al Kα source operating at 300 W. The base pressure was 2.7×10^{-8} Pa, and the operating pressure was 2.7×10^{-7} Pa. Charge compensation was accomplished using low energy electrons (−2.8 V bias voltage, −1.0 V filament voltage and a filament current of 2.1 A). Survey spectra were initially acquired at pass energy (PE) of 80 eV, followed by high-resolution spectra of Co2p, C.1s, O 1s and N 1s at PE of 20 eV for all of the samples. Acquisition times for survey C.1s and O 1s spectra were 20 min, F1s 5min for N 1s 2 scans of 20 min, and for Co2p 5 scans of 30 min. Data analysis and quantification

were performed using the CASAXPS software. A Shirley background was used for quantification and curve-fitting of Co2p spectra, while a linear background was used C.1s, N 1s and O 1s spectra. Quantification utilized sensitivity factors provided by the manufacturer. All the spectra were charge referenced to the aliphatic carbon at 285.0 eV. A 70% Gaussian/30% Lorentzian line shape was used for the curve-fits. The width of the individual peaks in the curve-fits for the Co2p, C.1s, and O 1s and N 1s spectra were constrained to a maximum of 1.4, 0.9, 1.3 and 1.0 eV respectively.

2.6. Multivariate analysis

Multivariate analysis of data was done using PLS_Toolbox 5.0 for Matlab. [15] Principal Component Analysis, using an autoscaling as a preprocessing option (mean centering and scaling to unit variance), was the default method of data analysis. PCA extracts the key mathematical principal components (PC) from a large data matrix by converting it into two smaller matrices that are easier to examine and interpret. The first PC accounts for the largest part of the variance in the data, the second PC accounts for the second-largest part of the variance, and so forth. The results of PCA are usually displayed as score plots (reflecting the significance of each sample in a principal component), loading plots (reflecting the significance of each variable in a principal component) and biplots (showing both samples and variables for two principal components). Biplots will be used herein as they provide a more instructive visualization of the groups of samples that are similar to each other and variables that are the most or least important for a specific sample group. Variables and samples that are highly correlated will be in the same region on a biplot [9].

3. Results and discussion

3.1. Electrochemical performance

Fig. 1 shows fuel cell polarization curves for five non-Pt cathode compositions. The best performing ink utilizes slow-cooled catalyst at 1:1 weight ratio of Nafion to catalyst. The performance of fuel cell utilizing the fast-cooled non-Pt catalyst material at the same ratio of 1:1 is quite similar to that of slow, while the increase of Nafion content caused a drop in performance.

Fig. 2 shows stability of the fast- and slow-cooled pyrolyzed non-Pt catalyst in an MEA configuration. The cathodes utilized the highest performing ink formulation of 1:1 at which current density as a function of time of operation at 0.4 V applied in hydrogen-air 80 °C, 206.8 kPa was measured. Even though the slow-cooled catalyst shows better initial performance, the fast-cooled catalyst shows better long-term stability for up to 750 h of operation. 1500 h of MEA operation is reported for the slow-cooled sample (data not shown).

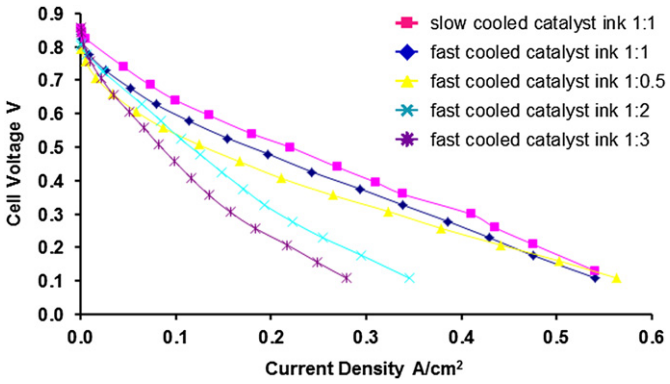

Fig. 1. H_2-air fuel cell polarization curves obtained for different non-Pt cathode electrode compositions.

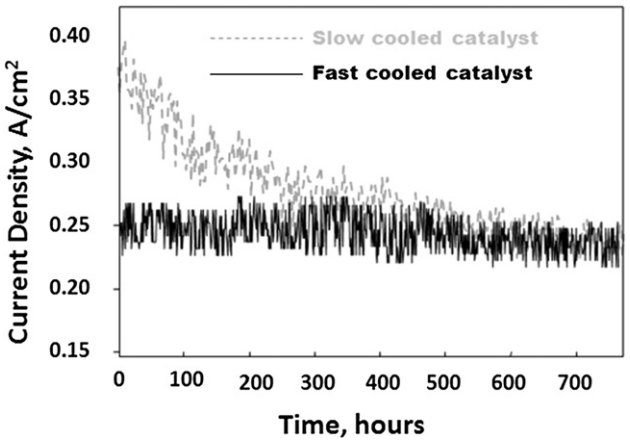

Fig. 2. Stability of fast- and slow-cooled CoTMPP catalysts in a MEA.

3.2. Morphology

The structure of the decorating cobalt phase on the catalyst surface may have practical implications in terms of the long-term stability of the non-platinum catalysts. For example, it is well known that transition metal oxides are predicted to be unstable in corrosive environments such as a PEM fuel cell. The geometric shape of the decorating phase could determine the longevity of the species based on dissolution rate and exposed surface area. TEM analysis of the CoTMPP catalysts is shown in Fig. 3. Two distinctive cobalt surface structures are observed in the magnified inserts. For slow-cooled catalysts insert a) shows the presence of cobalt surface particles in the size range of 5–10 nm. For fast-cooled catalysts insert b) shows the presence of dendrite-like structures. EDS–EDS (not shown) and XPS analysis (discussed later) of the same samples was also used to confirm identification of the particles as Co. We will discuss the effect morphology has on stability and activity of MEA in more detail below.

3.3. XPS characterization

Table 1 shows the elemental compositions for both slow- and fast-cooled catalyst powders and inks of various compositions as described in the Experimental section as well as that for carbon black powder and Nafion film as references. Both Nafion and Teflon modified carbon black contribute to the F signal. C and O have contributions from the CoTMPP catalyst, Nafion, and Carbon Black (CB), while N and Co come only from CoTMPP catalyst. The data shows the expected relative increase in %F as the Nafion concentration in the ink is increased.

Assuming a homogeneous mixture of all constituents of the ink, inks with a higher Nafion composition should show a decrease in the %Co and %N that are coming from catalysts only, while the Co/N ratio should remain unchanged. This is more or less valid for slow-cooled catalyst, but for the fast-cooled catalyst, the Co/N ratio is increasing ten-fold from lowest to highest Nafion contribution into the ink. Contrary to the expectations, as Nafion concentration increases in fast-cooled catalyst containing inks, total amount of Co detected also increases. It may be due to segregation of Co, which is, possibly, being leached from the catalyst by the Nafion, which is acidic in nature, to the very top surface.

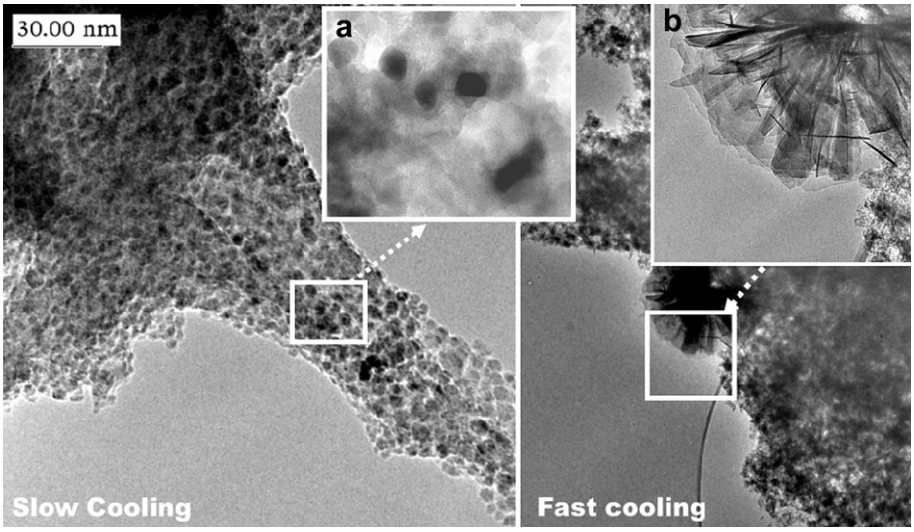

Fig. 3. TEM Micrographs of the slow and fast-cooled CoTMPP catalysts. Inserts a) and b) are magnifications of the cobalt particles and dendrite-like structures that form during pyrolyzation at 700 °C.

In order to confirm this hypothesis, long-term effect of Nafion on the structure of the catalyst in the fast-cooled containing inks was studied by retesting them after one month after storage in a refrigerator. Table 2 shows the elemental composition and Co/N ratio of the analyzed samples, fresh and stored. The Co/N ratio has increased by a factor of two. Leaching of Co by Nafion and its subsequent segregation to the very top surface is magnified by storage, and it is more significant for high content Nafion samples.

A more in-depth analysis was done by curve-fitting the high-resolution spectra to derive chemical speciation information for C, N, O, Co and F. Carbon black powder, CoTMPP powder and Nafion solvent-cast film were analyzed as references. Fig. 4 shows C, O and F high-resolution spectra for carbon black (CB) and Nafion, while Fig. 5 shows high resolution C, O, N and Co spectra for both slow and fast-cooled CoTMPP catalyst.

It is critical to know range of binding energy (BE) at which each of the constituents of the ink contributes in the spectra in order to distinguish any components that may be present due to intermolecular interactions between individual constituents. Table 3 shows curve-fit results for constituents shown in Figs. 4 and 5. C 1s of KB consists of 80% graphitic carbon with some amounts of surface oxides and some C–F species due to teflonization. The main peak for Nafion in the C 1s spectrum is at 291.2 eV due to CF_2–CF_2 main chain with minor contributions from higher BE components due to CF_3 side chains (292.6 eV) and CF_x–O at 293.9 eV. The peak assignment for the catalysts was based on our previous work in which evolution of species as a function of pyrolysis temperature of porphyrins was studied [16]. The main peak for both catalysts is due to the aliphatic carbon chain that comprises pyropolymer, with some amounts of unsaturated carbons, carbon that is bound to nitrogen and surface oxides. The amount of unsaturated carbon is much larger for fast-cooled catalyst than for slow-cooled one. Very significant overlap between various carbon-oxygen species, possibly C–O–F moieties, and Co oxides makes it very difficult to make sound conclusions on structure from O 1s spectra alone. The main peak in F 1s for carbon black is at 689.5 eV and is due to CF_3 moieties. A single peak in F is observed for Nafion due to the main CF_2–CF_2 chain.

A similar distribution of N species is observed for both catalysts. Similar amounts of N–Co and pyrrolic nitrogens are detected, with the major difference of higher amount of pyridinic N in slow- and higher amounts of quaternary-graphitic nitrogens in fast-cooled catalyst. Co speciation is quite different for slow- and fast-cooled catalyst. Fast-cooled catalyst has a much larger peak due to metallic and tricobalt tetraoxide components at 530.4 eV and less of Co associated with N than slow-cooled catalyst..

Fig. 6 shows C 1s spectra for fast-cooled catalyst containing inks as a function of increasing Nafion content, while Table 4 shows speciation for all elements for fast- and slow-cooled catalyst containing inks. Contributions of each peak were recalculated to the total atomic % of the element, so that each value in the table represents the actual amount in atomic % of the species. The discussion below refers to both absolute atomic % reported in

Table 1
Elemental compositions and ratios of CoTMPP catalyst inks determined by XPS (For inks, 1:x = Catalyst:Nafion).

	C 1s %	O 1s %	F 1s %	N 1s %	Co 2p %	Co/N
CB	89.4	2.2	8.5			
Nafion	29.3	8.2	62.5			
Slow-cooled						
Catalyst	80.5	12.4		5.8	1.30	*0.21*
Ink 1:0.5	44.5	7.0	47.0	1.3	0.20	*0.16*
Ink 1:1	30.6	6.4	62.4	0.5	0.09	*0.20*
Ink 1:2	29.4	6.5	63.4	0.5	0.17	*0.33*
Ink 1:3	29.5	6.1	63.7	0.6	0.06	*0.09*
Fast-cooled						
Catalyst	83.9	9.7	–	4.8	1.60	*0.33*
Ink 1:0.5	43.7	5.9	49.4	0.9	0.08	*0.09*
Ink 1:1	39.3	6.2	53.7	0.6	0.15	*0.23*
Ink 1:2	31.0	7.1	60.8	0.6	0.44	*0.71*
Ink 1:3	28.5	7.0	63.8	0.4	0.37	*0.98*

Table 2
Elemental composition for fast-cooled catalyst inks determined by XPS after one month of storage (For inks, 1:x = Catalyst:Nafion).

Sample	C 1s %	O 1s %	F 1s %	N 1s %	Co 2p %	Co/N
Ink 1:1 fresh	39.3	6.2	53.7	0.60	0.15	*0.23*
Ink 1:1 1 mo	44.3	6.4	48.3	0.70	0.30	*0.40*
Ink 1:3 fresh	28.5	7.0	63.8	0.40	0.37	*0.98*
Ink 1:3 1 mo	33.0	6.5	59.8	0.20	0.40	*2.00*

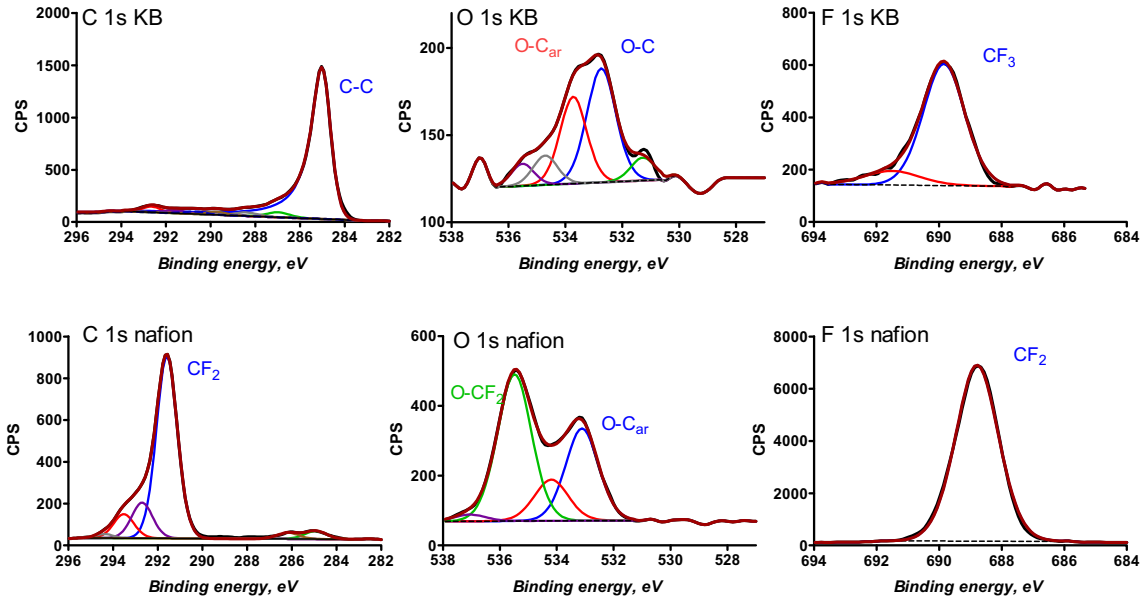

Fig. 4. C 1s, O 1s and F 1s high-resolution XPS spectra for teflonized carbon black (KB) and Nafion ionomer.

Table 4 as well as relative % each individual peak occupies within total signature of particular element, as both of these may show different trends. As the Nafion content increases we see an expected increase in high BE components of the C 1s spectra where Nafion contributes. The absolute % of this peak at 290.5 eV in the fast-cooled catalyst ink increases significantly but stays the same in slow-cooled catalyst ink. The main increase for both types of inks with increasing Nafion % is in the peak at a binding energy which is at lower BE than the main peak observed in Nafion. A shift of the BE may be caused by new types of species that are being formed as the result of intermolecular interactions between Nafion and catalyst and/or carbon black. For slow-cooled catalyst inks, this peak is at a BE of 289.8 eV, while for fast-quenched catalyst inks it is at slightly higher BE of 290.5 eV. The larger shift in BE from main Nafion peak for slow-cooled catalyst may indicate a larger degree of intermolecular forces such as hydrogen-bonds between moieties. Almost all aliphatic (saturated as well as unsaturated hydrocarbon) carbon species disappear for both types of inks.

O 1s shows significant differences between slow- and fast-cooled catalyst inks. For the slow-cooled catalyst inks a significant increase in the low BE part most probably due to Co_3O_4 is detected. For fast-cooled catalyst inks this peak at 530.4 eV does not exist at all, while relative (and absolute % in some degree) amounts of high BE components at 534.1 and 535.3 eV increase significantly with increase of Nafion concentration. This is at the BE range where O in pure Nafion exists, so we can suggest that this is due to O_yF_z types of moieties. This is also correlated with an increase in the C peak at 290.5 eV, which might be due to an $O_yC_xF_z$ species that form as result of the interaction of Nafion with carbon black and/or catalyst.

Very different behaviors are observed in the F 1s spectrum for both types of inks. As discussed above, pure Nafion has a major peak at 688.5 eV. The largest peak for slow-cooled containing catalyst inks is observed at 687.5 eV. The formation of this peak for both slow and fast-cooled catalyst containing inks indicates the formation of a new species. This peak is larger for slow-cooled catalyst containing inks, which also correlates with a larger shift in the BE of the C 1s spectrum of slow-cooled catalyst containing inks (298.8 eV) as compared to fast-cooled catalyst containing inks (290.5 eV). This may indicate an intermolecular bond between the Nafion and the catalyst and/or the carbon black with interactions being stronger for the slow-cooled catalyst. In fast-cooled catalyst containing inks, in addition to formation of this new peak, the increase in Nafion concentration causes an increase in the peak at 688.5 eV, which is due to the main Nafion peak as we would expect.

Except for the decrease in the overall amount of N for the slow-cooled catalyst containing inks as the amount of Nafion in them increases, the distribution of species does not change. For fast-cooled containing inks, the situation is quite different, i.e. almost all pyridinic N and Co—N peaks disappear as the Nafion amount increases and relative amounts of quaternary/graphitic nitrogens increase.

Changes in Co 2p for slow-cooled containing inks don't show any trend with increase of Nafion content. Absolute amounts of all types of Co decrease while the relative distribution stays similar from sample to sample. For fast-quenched catalyst containing inks the amount of metallic/tricobalt tetraoxide Co and Co—N decreases significantly as the Nafion content increases, and an increase in the amounts of high BE component peaks at 783.3 and 785.1 eV is observed. These are the BEs at which organometallic Co compounds are detected [17], so there is a possibility that the moiety that we have identified as one being formed in fast-cooled catalyst containing inks when catalysts is being mixed with Nafion, i.e. $O_yC_xF_z$, might be liganded to Co. So, most probably, this intermolecular component is between the Co part of the catalyst and Nafion, rather than between carbon black and Nafion, which is also confirmed by the total increase in Co concentration when Nafion % in the ink increases for the fast-cooled catalyst sample.

To get an additional insight into the trends between inks of different formulations and the types of species responsible for them, PCA was applied to the data in Table 4. Fig. 7 shows the PCA biplot obtained. The major variation in the data (52.2%) is captured by the first principal component which separates slow from fast-cooled containing inks. The second principal component which captures 22.1% of variance in the data separates high Nafion-containing samples from low. Both slow and fast-cooled containing inks are similar in composition when Nafion content is low (group I of samples and associated variables on biplot in Fig. 7). These samples have most species as present in pristine constituents preserved, i.e. carbon as in carbon black, most of the Co oxide, and

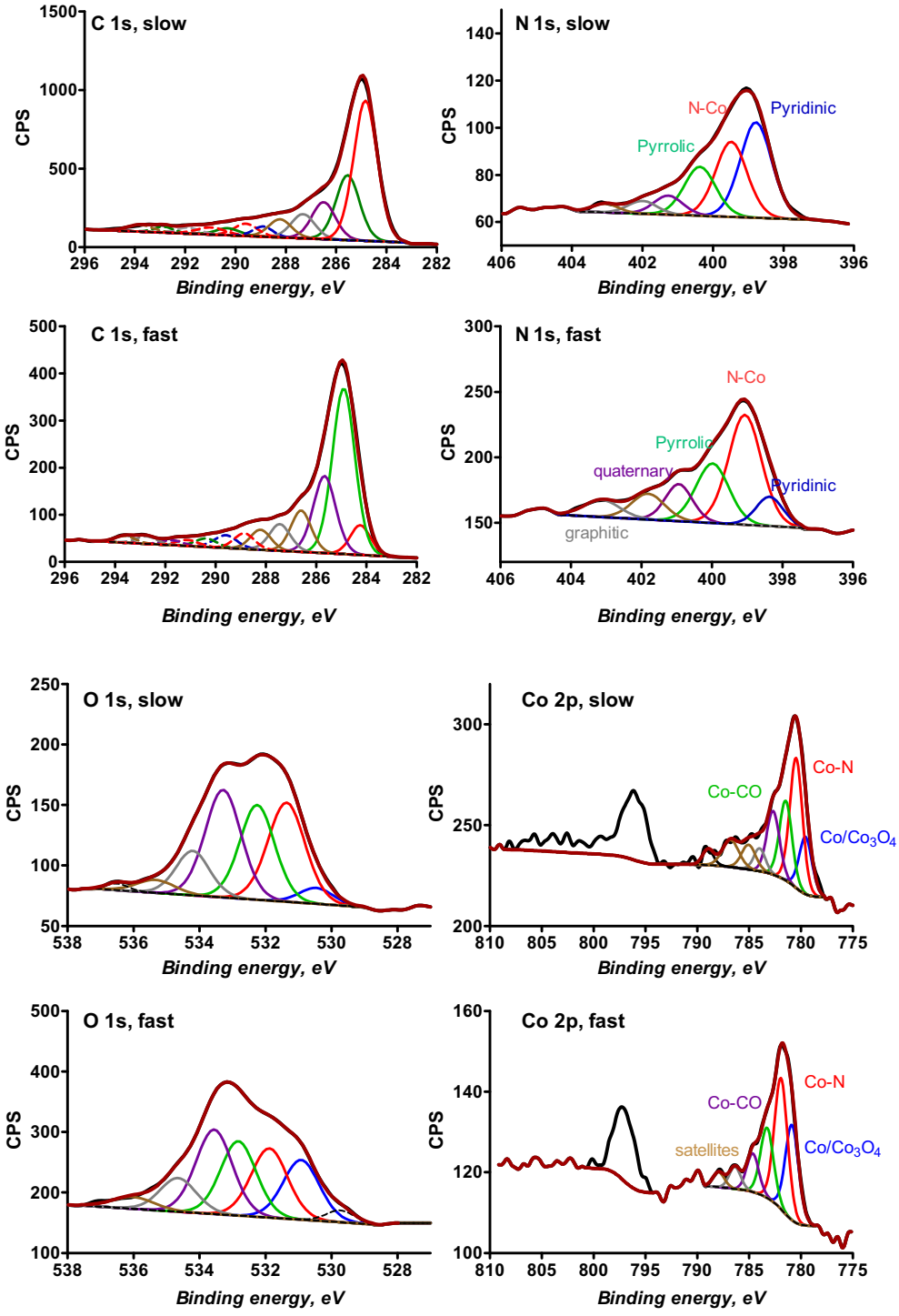

Fig. 5. C 1s, O 1s, N 1s and Co 2p XPS spectra for slow and fast-cooled catalysts.

C–F species and C–N species that are present in pure catalyst, carbon black and Nafion.

When the Nafion concentration is being increased in inks containing slow-cooled catalyst, it has little effect on the composition of the ink. 1:1, 1:2 and 1:3 slow inks are quite similar to each other and very different from all other samples, in having largest amounts of nitrogen bonded to Co, pyridinic nitrogen, F as present in Nafion, and C–O–F species as also are present in Nafion (group II on biplot in Fig. 7).

When the Nafion concentration is being increased in inks containing fast-cooled catalysts, big changes in composition are detected as captured by increased loading of inks with higher Nafion content into PC2 (group III on biplot in Fig. 6). Pyrrolic and graphitic nitrogen are dominant for high Nafion content fast-cooled catalyst inks. In addition, new and/or increase in peaks which are detected in F, C and Co confirm an interaction between the constituents of an ink resulting in the formation of new species such as Co–C–O–F.

Table 3
XPS speciation for individual constituents of inks (S = slow-cooled catalyst, F = fast-cooled catalyst).

	C 1s												
	C≡C, C–Co	C–C, KB	C–N	C–OH/C–OC	C–N_x	C=O/C–N=O	$C_xN_yO_z$/COOH		C–F	COOH/CF_2		CF_3/shakeup	CF_x–O
BE, eV	*284.1*	*285.0*	*285.7*	*286.6*	*287.5*	*288.3*	*289.1*	*289.8*	*290.5*	*291.2*	*291.9*	*292.6*	*293.9*
Carbon Black		82.8			2.9	2.8	2.8		2.2	2.0		4.6	
Nafion		3.2	0.7							72.2		12.4	11.5
S catalyst	6.2	40.5	18.5	9.6	7.1	4.9	3.5	3.3	2.2	1.5	1.0	1.6	
F catalyst	22.8	34.8	14.8	10.5	6.9	1.0	3.9	1.2		2.1	2.0		

	O 1s						F 1s		
	Co_3O_4	CoO, O=C	Co_2O_3/O–C al	O–C ar/O*–COCF	CNO	$Co(CO)_x$/O–CF2	CF_2–CF_2/O_2CF_3	CF_3	O_xCF_y
BE, eV	*530.4*	*531.3*	*532.3*	*533.3*	*534.1*	*535.3*	*688.5*	*689.5*	*691.5*
Carbon Black		6.1	41.1	31.6	16.0	5.2		86.5	13.5
Nafion				31.6	16.1	52.3	100.0		
S catalyst	5.2	26.7	25.0	30.2	13.8	4.3			
F catalyst	21.5	24.1	50.6	7.6	11.4	6.3			

	N 1s					Co 2p			
	Pyrid N	N–Co	Pyrrole N	Qua N	Graph N	Co/Co_3O_4	Co–N	$Co(CO)_x$ or Co–COF	
BE, eV	*398.8*	*399.5*	*400.4*	*401.1*	*402.0*	*780.7*	*781.9*	*783.3*	*785.1*
S catalyst	37.4	29.9	20.0	7.7	4.9	14.5	57.3	18.2	10.1
F catalyst	15.7	36.7	24.0	14.0	9.6	44.9	36.3	12.5	6.3

In order to understand the effect that cooling rate and Nafion concentration has on ink composition and stability, we have looked on how composition changes with respect to the species that are present in the original catalysts powders. For that, we have calculated the rates of change of each peak that is present in the catalyst and in the inks by computing the ratio of that peak in the ink to the corresponding peak in the catalyst powder. Table 1SI in the Supplementary Information shows the rate of change along with T which is the theoretical weight% of CoTMPP in the inks. A more meaningful and informative way to analyze these data is to compare and correlate the rates of changes of peaks/species to both the theoretical change in composition for the recipes and to each other, which is accomplished with PCA. The data in Table 1SI served as input for all subsequent principal component analyses aimed at showing correlations of the rates of decrease/destruction or increase/formation of the various species.

PCA biplot applied to data in Table 1SI in Fig. 8 shows a clear separation of slow and fast-cooled inks along principal component 1. Principal component 2 separates low from high Nafion content samples. T, the theoretical (i.e. by weight) % of catalyst in each recipe mixture, correlates with changes only for the lowest Nafion content samples for both slow- and fast-quenched containing inks (group I of samples and associated variables highlighted in biplot at Fig. 8). The species that follow theoretical

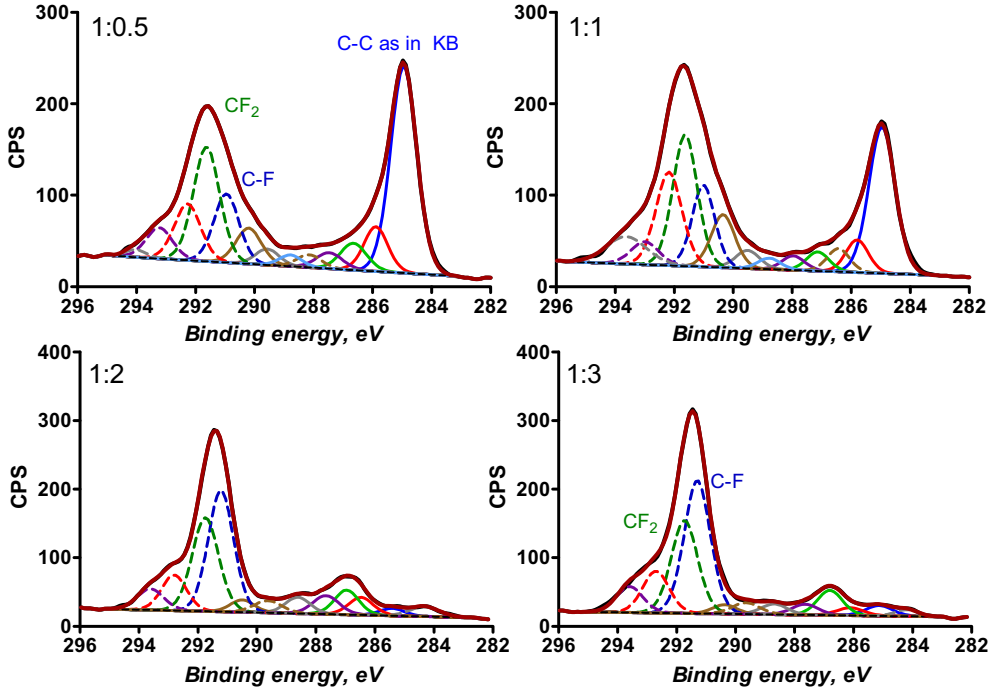

Fig. 6. C 1 s high resolution XPS spectra for fast-cooled catalyst containing inks of various Nafion content (Catalyst:Nafion).

Table 4
XPS speciation for inks and catalysts recalculated to sum of all species equal to 100% (F = fast-cooled catalyst ink, S = slow-cooled catalyst ink where 1:*x* = Catalyst:Nafion).

	Carbon 1s											
	C≡C, C–Co	C–C, KB	C–N	C–OH/C–OC	C–N_x	C=O/C–N=O	$C_xN_yO_z$/COOH		C–F	COOH/CF_2		CF_3/shakeup
BE (eV)	*284.1*	*285.0*	*285.7*	*286.6*	*287.5*	*288.3*	*289.1*	*289.8*	*290.5*	*291.2*	*291.9*	*292.6*
S catalyst	4.9	32.0	14.6	7.6	5.6	3.9	2.8	2.6	1.7	1.2	0.8	1.3
S 1:0.5	0.6	13.7	4.1	2.4	1.9	1.6	1.6	5.8	3.1	3.1	4.0	1.5
S 1:1	0.4	2.6	0.8	0.7	0.6	0.8	2.3	12.8	3.1	3.1	2.7	0.4
S 1:2	0.5	0.5	0.3	0.3	0.7	0.6	1.9	15.3	4.4	1.8	1.9	0.4
S 1:3	0.6	0.5	0.2	0.2	0.4	0.5	1.4	15.7	4.4	1.7	1.7	0.6
F catalyst	18.6	28.4	12.1	8.6	5.6	0.8	3.2	1.0	–	1.7	1.6	–
F 1:0.5	–	14.2	2.8	1.9	1.1	0.8	1.7	2.4	4.5	7.9	3.9	2.1
F 1:1	–	8.9	1.7	1.2	1.0	0.7	1.6	2.9	4.3	7.4	5.6	1.5
F 1:2	0.9	0.6	–	1.3	1.8	1.5	2.3	0.9	9.5	7.7	–	2.7
F 1:3	0.4	0.8	0.6	1.8	–	0.8	1.7	0.6	9.8	6.9	–	3.1

	Oxygen 1s						Fluorine 1s		
	Co_3O_4	CoO, O=C	Co_2O_3/O–C al	O–C ar/O*–COCF	CNO	$Co(CO)_x$/O–CF_2	F–CH_2	CH_2–CF_2/O_2CF_3	CF_2–CF_2–CF_2
BE (eV)	*530.4*	*531.3*	*532.3*	*533.3*	*534.1*	*535.3*	*687.5*	*688.5*	*689.5*
S catalyst	0.6	3.1	2.9	3.5	1.6	0.5	–	–	–
S 1:0.5	0.8	1.4	1.4	1.8	1.0	0.7	22.5	15.4	9.1
S 1:1	2.2	1.0	0.5	2.0	0.6	0.2	54.3	7.6	0.5
S 1:2	2.0	1.1	0.7	2.5	0.2	–	62.2	1.2	0.0
S 1:3	1.2	1.0	0.5	1.7	1.6	–	62.4	1.3	0.0
F catalyst	1.7	1.9	4.0	0.6	0.9	0.5	–	–	–
F 1:0.5	–	0.6	2.9	0.5	0.8	1.0	13.4	29.1	6.9
F 1:1	–	0.5	2.6	0.7	1.0	1.2	6.7	33.5	13.5
F 1:2	–	0.3	3.1	0.8	1.4	1.4	14.1	42.4	4.2
F 1:3	0.1	1.3	2.2	0.7	1.1	1.3	16.3	42.8	4.6

	Nitrogen 1s					Cobalt 2p			
	Pyrid N	N–Co	Pyrrole N	Qua N	Graph N	Co/Co_3O_4	Co–N	$Co(CO)_x$ or Co–F	
BE (eV)	*398.8*	*399.5*	*400.4*	*401.1*	*402.0*	*780.7*	*781.9*	*783.3*	*785.1*
S catalyst	2.13	1.70	1.14	0.44	0.28	0.19	0.74	0.24	0.13
S 1:0.5	0.21	0.47	0.36	0.19	–	0.03	0.10	0.05	0.03
S 1:1	0.14	0.13	0.10	0.04	–	0.03	0.03	0.02	0.01
S 1:2	0.12	0.11	0.10	0.09	0.05	0.05	0.03	0.06	0.04
S 1:3	0.16	0.22	0.11	0.03	0.05	0.01	0.03	0.01	0.01
F catalyst	0.74	1.73	1.13	0.66	0.45	0.72	0.58	0.20	0.10
F 1:0.5	0.08	0.21	0.25	0.20	0.10	0.02	0.03	0.01	0.01
F 1:1	–	0.17	0.11	0.17	0.06	0.00	0.06	0.04	0.05
F 1:2	–	–	0.09	0.19	0.11	0.00	0.07	0.22	0.15
F 1:3	–	0.02	0.07	0.07	0.12	0.00	0.05	0.15	0.17

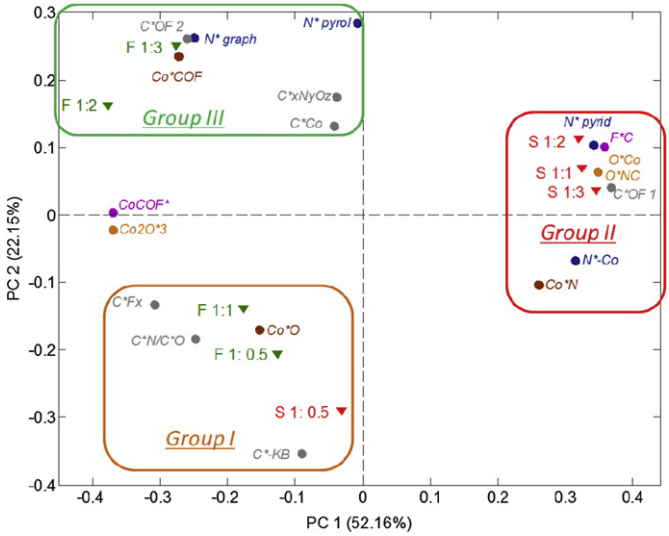

Fig. 7. PCA biplot for speciation results in Table 4 (F = fast-cooled catalyst ink, S = slow-cooled catalyst ink where 1:*x* = Catalyst:Nafion).

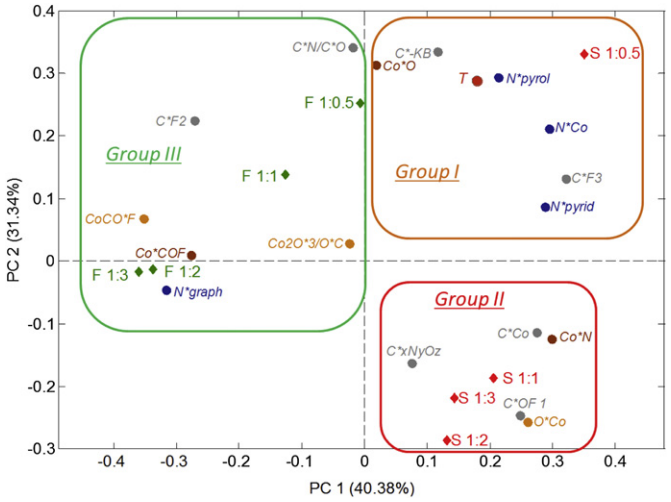

Fig. 8. PCA biplot for rates in Table 1SI (F = fast-cooled catalyst ink, S = slow-cooled catalyst ink where 1:*x* = Catalyst:Nafion).

changes are N species, i.e. pyridinic, pyrrolic, N–Co, carbon as in carbon back, CoO and C–F_3 as in Nafion. Changes in Co*–N do not correspond to theoretical composition and have higher prevalence in slow-cooled high Nafion content inks. This would be consistent with attributing changes in the Co/N ratio as a function of Nafion content to a change on the Co rather than a change in the N. Slow-cooled high Nafion-containing inks are clustered together and having highest contribution due to CNO species and oxidized species C–O–F as present in Nafion as well as Co–N peak (group II in biplot).

On the left part of the PC biplot (group III), all fast-cooled inks have contributions from all high binding energy components in Co, O and C. The formation of intermolecular bonds between Nafion and catalysts and carbon black, which results in Co–C–O–F type of moieties, is accompanied by the formation of graphitic/quaternary nitrogens.

3.4. Structure-to-property correlations

Fig. 9 shows PCA for subset of samples for which MEA testing was performed as shown in Fig. 1. Lower Nafion content samples have higher currents *I* which are associated with unoxidized F*–C and C*–F in Nafion, carbon in carbon black (C*KB) and C*–O–F as in pristine Nafion. The significance of nitrogen associated with metal is confirmed by both N and Co respective species. Pyridinic N and the lowest BE component of O is also correlated with better MEA performance. Stability of the inks, which is higher for fast-cooled catalyst samples F 0.5 and F 1, is thus associated with presence of graphitic carbon and unoxidized C–F species while performance, which is the same for S 1, F 0.5 and F 1 samples, is linked to pyridinic N and N associated with metal as reported by us before.

Fast-cooled samples with higher Nafion content result in both worse performance, which is reflected by lower currents as well as worst stability. Higher concentrations of Nafion causes leaching of metal from the nitrogen carbon network and the oxidation of the Nafion backbone itself resulting in the formation of oxidized Co–C–O–F species and graphitic nitrogen.

The shape of nanostructured materials has a significant impact on their properties [18,19]. Morphologies of “nano-flowers” or dendritic structures as shown in Fig. 3b exhibit hierarchical structures behavior with different ordered units in spatial direction and with different levels of roughnesses at different length scales. Advantageous electrochemical surface area and related to its high catalytic activity has been reported for Cobalt hexacyanoferrate [20].

Chemical and structural changes during degradation process that we have discussed in terms of chemical speciation as determined by XPS will be accompanied by morphological changes. The loss of surface area of active sites is the major contributing factor in the observed loss of performance. Geometry of the particles is responsible for the relative loss of surface area, i.e. spheroidal structure as present in the nano-particles decorating the slow-cooled catalyst (Fig. 3a) being more susceptible to such loss than dendritic, branched hierarchical structure as displayed by the decorating phase in the fast-cooled catalyst (Fig. 3b). Therefore, fast-cooled (quenched) catalyst is more stable then slow-cooled catalyst as confirmed by structure-to-property correlations shown in Fig. 9.

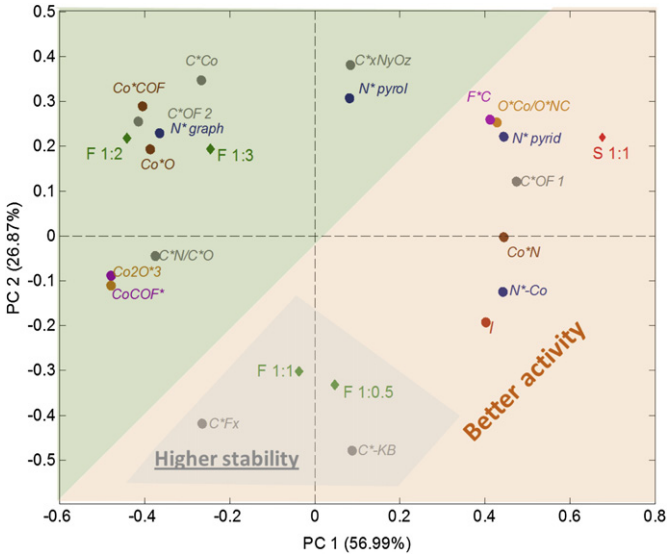

Fig. 9. PCA biplot for XPS and MEA test data combined. Low Nafion content fast- and slow-cooled catalyst inks have higher currents I then high Nafion content samples (F = fast-cooled catalyst ink, S = slow-cooled catalyst ink where 1:*x* = Catalyst:Nafion).

4. Conclusion

Different formulations of CoTMPP-containing inks were tested in a fuel cell MEA configuration and analyzed by XPS and multivariate analysis. Fast and slow-cooled catalyst powders were used with various amounts of Nafion to study effect of leaching time trajectories and Nafion content on stability as well as MEA performance.

Large changes in Co/N ratios with an increase of Nafion content in the ink formulation were observed. The arrangement of Co chemical environment changes dramatically with increasing Nafion concentrations, especially for fast-cooled catalyst inks. Co oxide almost completely disappears in all fast-cooled catalyst inks, while it is still present for slow-cooled catalyst inks. The Co that is being extracted from the catalyst mostly from CoO is being converted to a mixture of Co, F, O and C. No N is associated with these new types of species, and Co–N stays intact and present at stoichiometric amounts expected for each ink formulation.

By building structure-to-property relationships between XPS and MEA testing data using PCA we have determined that the higher stability of fast-quenched inks is mainly associated with better preserved graphic carbon from the carbon black and C–F moieties of the Nafion, while better MEA performance is a convolution of presence of these moieties as well N in pyridinic form and N associated with metal in the pyropolymer. Optimal Nafion content is determined as 1:1, while higher Nafion concentrations cause oxidation of the Nafion backbone itself as well as leaching of the CoO particles from catalyst, which was suggested to be the second active site for ORR, therefore resulting in worse MEA performance [21].

Acknowledgments

We would like to acknowledge the support of DOE-EPSCoR DE-FG02-08ER46530 New Mexico Implementation Program and IGERT fellowship program.

Appendix A. Supplementary data

Supplementary data related to this article can be found at http://dx.doi.org/10.1016/j.jpowsour.2012.10.062.

References

[1] R. Jasinski, J. Electrochem Soc. 112 (1965) 526.
[2] F. Jaouen, F. Charreteur, J.P. Dodelet, J. Electrochem Soc. 153 (2006) A689–A698.
[3] F. Jaouen, J.P. Dodelet, J. Phys. Chem. C 111 (2007) 5963–5970.
[4] Z.F. Ma, X.Y. Xie, X.X. Ma, D.Y. Zhang, Q.Z. Ren, N. Hess-Mohr, V.M. Schmidt, Electrochem Commun. 8 (2006) 389–394.
[5] T.S. Olson, K. Chapman, P. Atanassov, J. Power Sources 183 (2008) 557–563.
[6] M. Yuasa, T. Kondo, D. Mori, S. Arikawa, Polym. Advan. Technol. 22 (2011) 1235–1241.
[7] D.C. Huang, P.J. Yu, F.J. Liu, S.L. Huang, K.L. Hsueh, Y.C. Chen, C.H. Wu, W.C. Chang, F.H. Tsau, Int. J. Electrochem Sc 6 (2011) 2551–2565.
[8] H.A. Gasteiger, S.S. Kocha, B. Sompalli, F.T. Wagner, Appl. Catal. B-Environ 56 (2005) 9–35.
[9] K. Artyushkova, S. Pylypenko, M. Dowlapalli, P. Atanassov, J. Power Sources 214 (2012) 303–313.
[10] K. Artyushkova, S. Pylypenko, M. Dowlapalli, P. Atanassov, RSC Adv. 2 (2012) 4304–4310.
[11] V. Parry, G. Berthome, J.C. Joud, O. Lemaire, A.A. Franco, J. Power Sources 196 (2011) 2530–2538.
[12] J. Xie, D.L. Wood, K.L. More, P. Atanassov, R.L. Borup, J. Electrochem Soc. 152 (2005) A1011–A1020.
[13] F.Y. Zhang, S.G. Advani, A.K. Prasad, M.E. Boggs, S.P. Sullivan, T.P. Beebe, Electrochim. Acta 54 (2009) 4025–4030.
[14] C. Chen, G. Levitin, D.W. Hess, T.F. Fuller, J. Power Sources 169 (2007) 288–295.
[15] I. Eigenvector Research, in, Wenatchee, WA.
[16] K. Artyushkova, S. Levendosky, P. Atanassov, J. Fulghum, Top. Catal. 46 (2007) 263–275.
[17] NIST Standard Reference Database 20, Version 3.5 (2007).
[18] M.K. Roy, B. Haldar, H.C. Verma, Nanotechnology 17 (2006) 232–237.
[19] H. Heli, M. Hajjizadeh, A. Jabbari, A.A. Moosavi-Movahedi, Anal. Biochem. 388 (2009) 81–90.
[20] H. Heli, I. Eskandari, N. Sattarahmady, A.A. Moosavi-Movahedi, Electrochim. Acta 77 (2012) 294–301.
[21] K. Artyushkova, S. Pylypenko, T.S. Olson, J.E. Fulghum, P. Atanassov, Langmuir 24 (2008) 9082–9088.